Geochemical indicators of metalliferous fertility in the Carboniferous San Blas pluton, Sierra de Velasco, Argentina

J. N. Rossi, A. J. Toselli, M. A. Basei, A. N. Sial and M. Baez

Geological Society, London, Special Publications 2011; v. 350; p. 175-186
doi:10.1144/SP350.10

Geochemical indicators of metalliferous fertility in the Carboniferous San Blas pluton, Sierra de Velasco, Argentina

J. N. ROSSI[1]*, A. J. TOSELLI[1], M. A. BASEI[2], A. N. SIAL[3] & M. BAEZ[1]

[1]*Facultad de Ciencias Naturales, UNT. Miguel Lillo 205, CP. 4000, Tucumán, Argentina*

[2]*Instituto de Geociencias, Universidade de São Paulo, Rua do Lago 562, São Paulo, Brazil*

[3]*NEG-LABISE, Department de Geologia, Universidade Federal de Pernambuco, C.P. 7852, Recife, PE, 50670-000, Brazil*

**Corresponding author (e-mail: juanitarossi@gmail.com)*

Abstract: In the Sierra de Velasco, northwestern Argentina, undeformed Lower Carboniferous granitoids (350–334 Ma) intrude deformed Lower Ordovician granites and have been emplaced by passive mechanisms, typical of tensional environments. The semi-elliptic, about 300 km^2 shallow-emplaced San Blas pluton is 340–330 Ma old, with εNd_t between −1.3 and −1.8 which indicates that, different from the nearby Famatinian–Ordovician granitoids, the San Blas pluton had a relatively brief crustal residence, with an interaction between asthenospheric material and greywackes. The cupola of the pluton was almost totally eroded down during the Upper Carboniferous.

The San Blas pluton is a porphyritic granite composed mainly of monzogranite to syenogranite and shows graphic intergrowth and miarolitic cavities up to 5 cm in diameter, filled with quartz. Two different textures are recognized: perthitic microcline megacrysts (30–45 vol%) set in a medium- to coarse-grained groundmass of quartz, microcline and oligoclase, with sericitic alteration. Biotite, muscovite, apatite, zircon, fluorite and opaque minerals are the accessory phases. The other textural variation consists in microcline megacrysts (10%–15 vol%) and a fine-grained groundmass, of quartz, microcline and oligoclase, biotite, apatite, muscovite, zircon and magnetite.

The average SiO_2 content in this pluton is 74.94%, the ASI = 1.1, CaO and MgO are less than 1%, total Fe_2O_3 and P_2O_5 contents are low, and $K_2O > Na_2O$. Low Ba, Sr and high Rb contents, coupled with Sn contents (*c.* 15 ppm), W (*c.* 380 ppm), Nb, Y, Ta, Th and U confirm this is a special granite. The K/Rb ratio (*c.* 75) indicates that Rb has been fractionated to the residual melt whereas the Zr/Hf (*c.* 25) demonstrates that hydrothermal alteration occurred. The Sr/Eu ratio of *c.* 75 along other geochemical features characterize this pluton as a fertile evolved granite.

The chondrite-normalized rare earth element (REE) diagram shows the tetrad effect that allows the subdivision of the lanthanides into four groups.

In general, the tetrad effect is recognized in evolved granites and products of hydrothermal alteration such as greisens. The above-mentioned features show that the San Blas granite is fertile, and the absence of ore deposits has been probably caused by erosion of a mineralized cupola during Carboniferous and Cenozoic exhumation. The finding of alluvial cassiterite and wolframite in drainage systems is the first evidence of the fertile character of this granite.

At the Sierra de Velasco, extensive exposures of Lower Ordovician, I- and S-type granitoids are observed. They are mainly syn- to late- and post-kinematic, and are now orthogneisses of the Famatinian orogenic cycle, a wide magmatic arc in northwestern Argentina (Pankhurst *et al.* 2000; Toselli *et al.* 2002, 2007). Ordovician to Devonian deformation bands and NW–SE trending lineaments have affected the whole geological setting (Toselli *et al.* 2007).

In the northern and central parts of the Sierra de Velasco, these granitoids are intruded by three bodies of mainly Lower Carboniferous age, the Sanagasta, Huaco and San Blas plutons. The deformation structures are crosscut by some of these younger plutons.

The Huaco and Sanagasta granitoids are two adjacent sub-ellipsoidal, undeformed plutons (Grosse *et al.* 2009), and the San Blas pluton is a notable semi-elliptic shaped granite (Báez 2006).

The three granites share common features, being porphyritic monzo- to syeno-granites which are geochemically evolved with SiO_2 contents between 73 and 75%.

From: SIAL, A. N., BETTENCOURT, J. S., DE CAMPOS, C. P. & FERREIRA, V. P. (eds) *Granite-Related Ore Deposits.* Geological Society, London, Special Publications, **350**, 175–186.
DOI: 10.1144/SP350.10 0305-8719/11/$15.00

The main objective of this contribution is to discuss in detail the field relationships, petrography, mineralogy, geochemical evolution and fractionation of the San Blas pluton (Fig. 1). The potential metalliferous fertility of this pluton will be also considered. Lannefors (1929) and some unpublished reports of the Mining and Geological Survey of Argentina indicate the finding of alluvial cassiterite and wolframite in drainage systems developed within this pluton. It was the first evidence of a fertile character in this granitic pluton.

Rb–Sr and Sm–Nd isotopic data are used to determine crustal residence age, the origin and possible contribution from juvenile material to allow a comparison with nearby Ordovician granitoids of the Pampean Ranges.

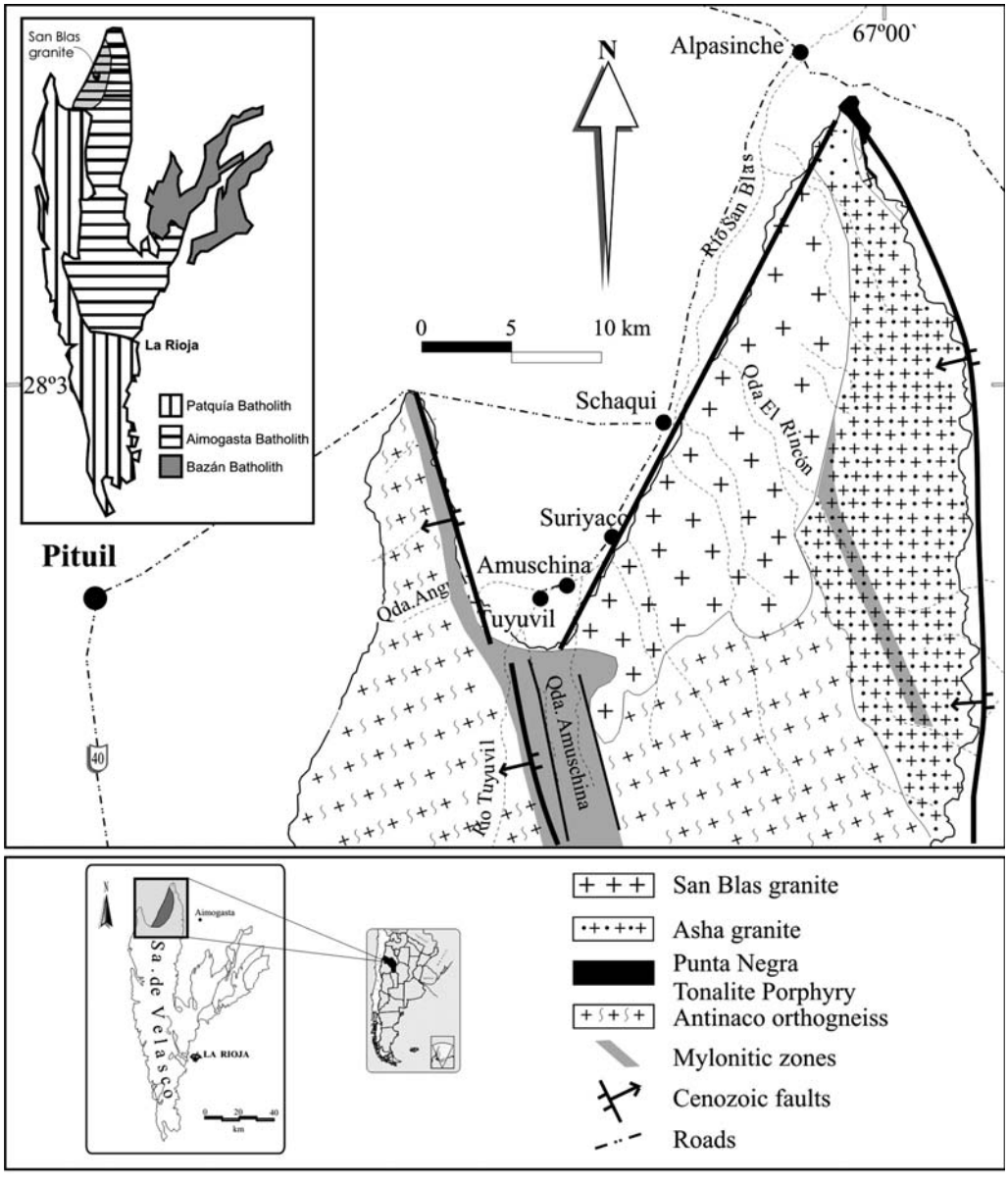

Fig. 1. Geological sketch of the Sierra de Velasco and San Blas Granite, northwestern Argentina.

Analytical techniques

Major elements were determined by inductively coupled plasma - atomic emission spectroscopy (ICP-AES), and trace elements by inductively coupled plasma mass spectrometry (ICP-MS) at the Activation Laboratories (Canada), using lithium metaborate/tetraborate fusion.

Isotopic analyses were performed at the Zentrallabor für Geochronologie des Departments für Geo- und Umweltwissenschaften der Ludwig Maximilians Universität, Munich. Powdered samples for Rb–Sr and Sm–Nd analyses were dissolved in a mix of HF, HNO_3 and $HClO_4$. Before dilution, samples for Rb and Sr analyses were treated separately with a spike. Chemical separation of Rb and Sr used cation exchange technique on DOWEX AG 50Wx8 resin. Isotopic ratio measurements were made with Finnigan THQ mass spectrometer. The measured isotopic ratios were normalized to $^{88}Sr/^{86}Sr = 8.3752094$.

For Sm and Nd, samples were treated with a combined Sm–Nd–Sr spike. The separation of the REEs was performed with cationic exchange techniques using DOWEX AG 50W×8 resin. The separation of Sm from Nd was done using with the H_3PO_4 HDEHP ester on teflon powder as the cation exchange resin. The isotopic ratios were normalized to $^{146}Nd/^{144}Nd = 0.7219$. Isotopic ratio measurements were performed in a MAT 261/262 mass spectrometer, with a confidence interval of 95% (2σ).

Geological and petrographic characteristics

The San Blas body is a semi-elliptic pluton about 28 km long and 8 km wide, located to the north of the Sierra de Velasco, with its major axis trending NE–SW (Figs 1 & 2a).

The surface morphology shows a smooth westward tilted erosion surface exposed since the Upper Carboniferous (Jordan & Allmendinger 1986). At the southwestern boundary, this pluton intrudes the Ordovician Antinaco orthogneiss, and contains incorporated xenoliths of the country rock; northwards it intrudes the Ordovician Punta Negra porphyry tonalite (Fig. 1), and to the east it shows sharp contacts against the supposedly Ordovician La Costa pluton (Toselli *et al.* 2006). The absence of deformation at its contacts zones and the incorporation of xenoliths by stopping suggest for the San Blas granite a post-tectonic passive intrusion mechanism in a brittle shallow setting.

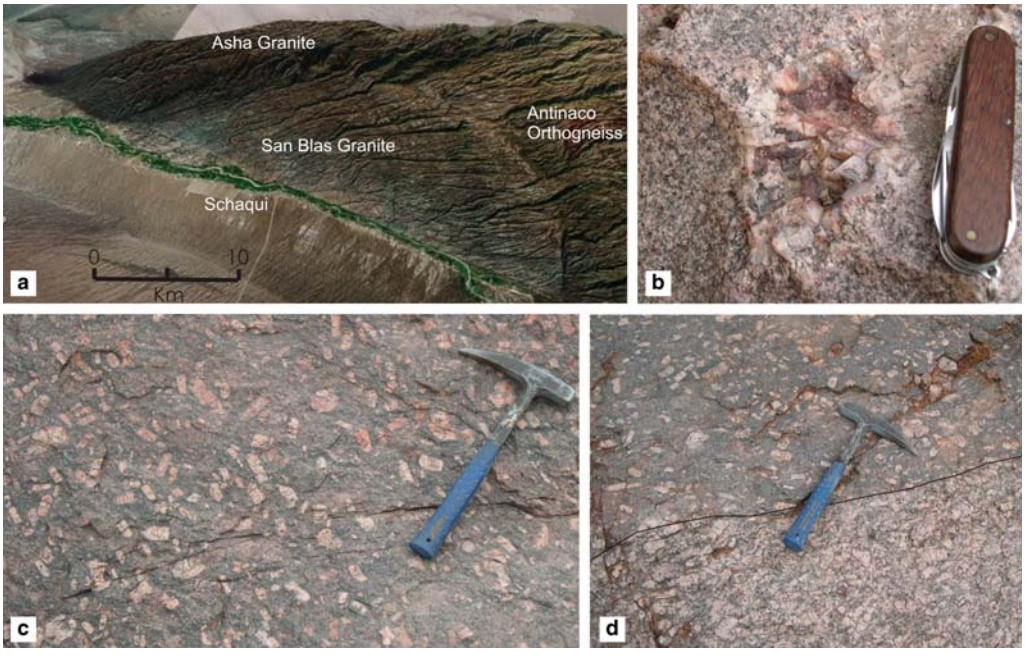

Fig. 2. (**a**) Panoramic overview of the outcrop of the San Blas pluton and its Carboniferous erosion surface; (**b**) miarolitic cavities; (**c**) microcline megacrysts in a fine-grained groundmass; (**d**) contact zone between medium- to coarse-grained granite and fine grained matrix with megacrysts.

Table 1. *Whole rock chemical analysis. Major elements in %. Traces in ppm*

Sample	5795	6336	6340	6445	6447	6452	6511	6513	6514	6515	6523	6749	6754
SiO_2	75.20	70.78	73.93	73.73	75.71	75.23	75.47	76.59	74.45	76.86	75.26	74.93	76.11
TiO_2	0.10	0.34	0.22	0.12	0.12	0.21	0.17	0.10	0.07	0.02	0.19	0.03	0.12
Al_2O_3	12.39	14.31	13.24	14.74	13.15	12.63	12.65	12.71	12.29	13.08	13.07	14.64	12.40
Fe_2O_3t	1.44	2.80	1.99	1.23	1.46	2.02	1.88	1.27	1.60	0.40	1.88	0.60	1.76
MnO	0.04	0.05	0.03	0.13	0.04	0.03	0.04	0.05	0.04	0.07	0.09	0.12	0.03
MgO	0.07	0.32	0.12	0.18	0.24	0.14	0.09	0.22	0.02	0.07	0.09	0.12	0.03
CaO	0.60	1.16	0.66	0.69	0.62	0.60	0.74	0.48	0.77	0.37	0.52	0.32	0.63
Na_2O	3.16	3.48	3.11	3.80	2.92	2.95	3.15	2.88	3.69	4.53	2.93	4.12	2.89
K_2O	4.82	5.78	5.78	4.37	4.68	5.46	4.90	4.05	4.88	4.30	4.52	3.76	5.53
P_2O_3	0.02	0.19	0.10	0.28	0.13	0.09	0.06	0.15	0.02	0.06	0.10	0.30	0.03
LOI	0.99	1.05	1.06	1.14	1.31	0.81	1.04	0.95	1.00	0.52	1.06	0.67	0.86
Total	98.33	100.26	100.24	100.41	100.38	100.18	100.18	99.44	98.83	100.21	99.78	99.51	100.40
Rb	583	594	460	465	473	446	496	426	771	576	395	689	546
Sr	19	66	56	29	18	38	34	21	8	16	46	28	18
Ba	46	179	188	95	37	121	128	36	20	36	203	20	73
Zr	103	284	231	51	59	200	227	50	211	70	153	18	167
Cs	n.a.	39.2	18.4	61.2	21.4	16.7	40.6	37.7	41.2	22.2	19.6	13.3	21.7
Hf	4.90	8.4	6.7	2.00	2.1	5.5	7.5	1.9	11.9	6.4	5.3	1.2	6.5
Y	88	72	37.4	23.1	25.7	54	61.6	23	192	58	63	3	89
Nb	74.0	47.2	34.9	25.5	9.7	25.1	43	10.7	102	48.8	31.0	25.2	64.5
Ta	14.70	14.2	9.75	10.2	4.29	6.31	13.6	8.00	17.3	33	6.74	14.0	11.6
Ga	26	27	23	22	12	22	24	15	35	35	16	20	29
Th	50.80	49.5	40.6	11.20	7.18	87.1	60.8	6.43	97.6	18.3	46.0	4.15	57.6
U	17.0	5.11	7.69	4.62	2.10	8.60	6.63	3.01	10.4	2.53	10.3	5.22	18.8
Sn	16	21	14	9	6	10	14	13	20	8	17	2	6
W	320	568	609	490	254	305	579	284	595	325	242	177	178

Table 2. *Lanthanides, K, Rb, Sr, Zr and Hf of San Blas granite. C_1 Chondrite of Sun & McDonough (1989). Data in ppm*

Sample	5795	6445	6447	6452	6511	6513	6514	6515	6523	6749	6754	C_1
La	35.60	13.2	8.93	89.9	44.3	6.92	44.2	23.9	38.2	1.37	53.2	0.237
Ce	82.90	28.0	20.5	1.97	94.6	17.2	108	63.9	86.8	2.87	120	0.612
Pr	9.24	3.47	2.35	20.6	11.7	2.05	13.4	7.82	9.70	0.30	14.4	0.095
Nd	39.10	12.2	8.74	69.4	40.3	7.46	56.4	28.3	34.9	1.06	56.1	0.467
Sm	10.60	3.09	2.43	12.8	9.33	2.29	16.0	8.52	8.22	0.23	12.6	0.153
Eu	0.25	0.41	0.205	0.58	0.66	0.172	0.17	0.12	0.61	0.01	0.49	0.058
Gd	10.70	2.65	2.54	9.26	8.0	2.21	17.2	7.84	7.36	0.19	12.2	0.2055
Tb	2.39	0.62	0.63	1.66	1.73	0.58	3.88	1.96	1.64	0.04	2.32	0.0374
Dy	15.0	3.89	4.15	9.85	10.8	3.73	25.5	13.3	10.2	0.33	14.8	0.2540
Ho	2.97	0.76	0.82	1.82	2.08	0.74	5.78	2.68	2.03	0.07	3.07	0.0566
Er	10.0	2.22	2.74	5.34	5.85	2.47	17.6	9.85	6.39	0.27	9.71	0.1655
Tm	1.67	0.42	0.479	0.783	0.98	0.464	2.89	1.95	0.97	0.06	1.55	0.0255
Yb	10.20	2.77	3.20	4.68	5.74	3.27	17.6	15.4	6.21	0.55	9.96	0.170
Lu	1.41	0.40	0.491	0.631	0.79	0.518	2.48	2.51	0.91	0.01	1.41	0.0254
K	40012	36277	38850	45325	40675	33619	40510	35696	37525	31216	45910	545
Rb	583	465	473	446	496	426	771	576	395	689	546	2.32
Sr	19	29	18	38	34	21	8	16	46	28	18	7.26
Zr	103	51	59	200	227	50	211	70	153	17	167	3.87
Hf	4.90	2.0	2.1	5.5	7.5	1.9	11.9	6.4	5.3	1.2	6.5	0.1066

The western boundary, covered by modern sediments, is sharply defined by a north–southward trending fault (Figs 1 & 2a).

The San Blas pluton is composed essentially of porphyritic monzogranites and, less often, of syenogranites. Within the borders and in the central area, semi spherical miarolitic cavities have been recognized, up to 5 cm sized, some of them filled with quartz crystals and others contain graphic intergrowth of quartz and microcline (Fig. 2b).

Two textural phases have been recognized: (*a*) a fine grained groundmass with scarse phenocrysts content, at the northeastern and southwestern borders, and (*b*) a medium- to coarse-grained groundmass with abundant phenocrysts in the central zone of San Blas pluton. There is no sharp textural transition between the two phases which appear to be intermingled sometimes (Fig. 2c, d).

In the phase *b*, perthitic microcline megacrysts constitute 30–45% of the total volume of the rock. They are tabular shaped, euhedral to subhedral, from 3 to 15 cm long, and often contain inclusions of biotite and quartz.

In thin section, the groundmass of the porphyritic granite is inequigranular, medium- to coarse-grained. It is composed of quartz, microcline and oligoclase with some alteration to sericite. Biotite, in higher modal content than muscovite, is flake-shaped (1–3 mm long), shows corroded borders and appears in clusters associated with opaque minerals. Accessory minerals are apatite in round-shaped grains and subhedral zircon. Fluorite is interstitial and relatively scarce.

In some places, the abundance of microcline megacrysts decrease to 10% and the groundmass changes to a more fine-grained nearly aplitic texture and the fluorite being more abundant and secondary muscovite increases. In these weakly altered zones, neither topaz nor tourmaline has been found. Zircon grains are prismatic shaped (0.01–0.04 mm long).

The phase *a* contains less microcline megacrysts (10%–15 vol%) set in a fine-grained inequigranular groundmass (0.2–1 mm). Megacrysts are euhedral to subhedral, 1 to 5 cm long, often exhibiting Carlsbad twins. In thin sections, microcline displays albite–pericline twins, and often inclusions of biotite and quartz. The groundmass is composed of quartz, microcline, sodic oligoclase as essential minerals and apatite, muscovite, zircon and magnetite as accessory minerals.

Geochemistry

Whole-rock major, minor and trace chemistry data are presented in Tables 1 and 2. The content of SiO_2: (71–76%) has a mean value of 74.9%; TiO_2, CaO and MgO are lower than 1%; Fe_2O_{3total}: (0.4–2.8%) has a mean value of 1.56%; $K_2O > Na_2O$, with a mean value $K_2O < 5\%$. P_2O_5 contents are low (average value around 0.12%). All of these data suggest significantly evolved granite magma. The aluminum average of saturation index (ASI = molar $[Al_2O_3/(CaO + Na_2O + K_2O)] = 1.10$) indicates moderate peraluminosity (Fig. 3).

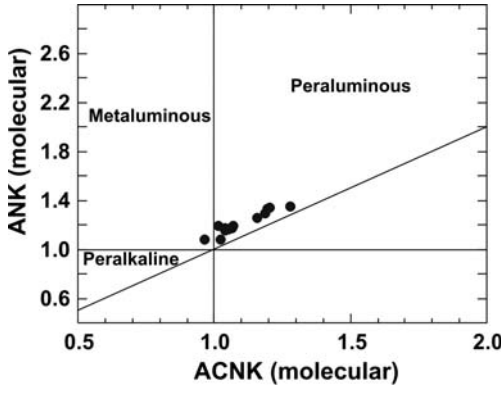

Fig. 3. ($Al_2O_3/CaO + Na_2O$) v. ACNK ($Al_2O_3/CaO + Na_2O + K_2O$), from Maniar & Piccoli (1989). Granite samples plot mainly in the peraluminous field.

The trace element chemistry points to high evolution of the San Blas pluton better than major elements. A low mean content for Ba (77 ppm), Sr (31 ppm), high average value content of Rb (532 ppm) and of Cs (29.4 ppm) are observed but even so the HFSE (Nb, Ta and Y) have high average values. Th and U contents are also high and indicate their fractionation in REE, Y, Th, U-rich accessory minerals as monazite, zircon and apatite (Bea 1996). High content of Sn (mean value 12 ppm) and W (mean value 379 ppm) confirms the specialized character of the San Blas granite (Table 1).

The K/Rb ratio has been used to characterize the evolution state of granitic melts. $K/Rb < 100$ ratios are regarded as indication of highly evolved granitic melts. The mean value of $K/Rb = 76$ indicates that Rb tends to fractionate in residual melt or the fractionation between a silicate melt and an aqueous fluid phase (Clarke 1992); the mean value of $Zr/Hf = 24$ is lower than the chondritic ratio (36.4). $Zr/Hf < 20$ ratios are characteristic for strong magmatic – hydrothermal alteration (Irber 1999). Recently, Bea *et al.* (2006) have demonstrated that Zr/Hf significantly lower than chondrite results from zircon fractionation.

Sr/Eu ratio ranges from 37 to 138, with an average value of 77, being most values lower than the chondritic ratio (125). The observed range suggests fractionation of both, Sr and Eu^{2+} and so

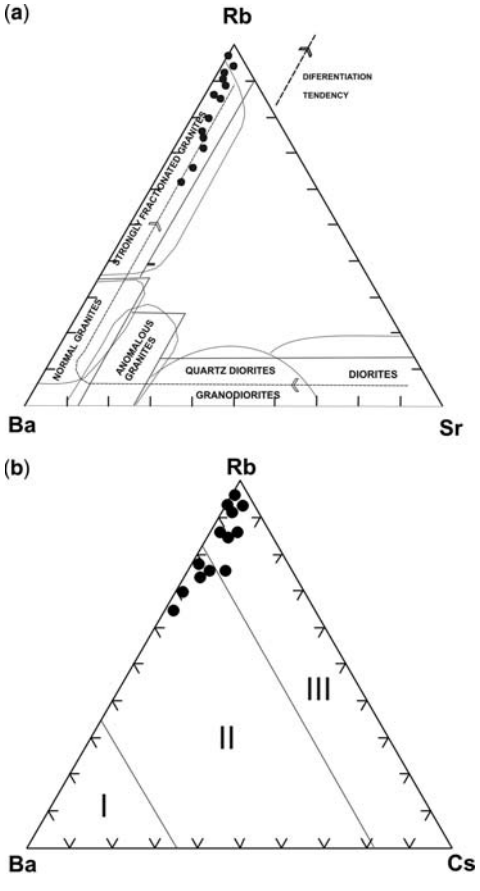

Fig. 4. (**a**) Rb–Ba–Sr plot (El Bouseily & El Sokkary 1975). Plotted points shift to strongly differentiation granites; (**b**) Rb–Ba–Cs plot (El Bousely & El Sokkary 1975), granites plot in fields II and III that indicate different potentials of mineralization of Sn and W.

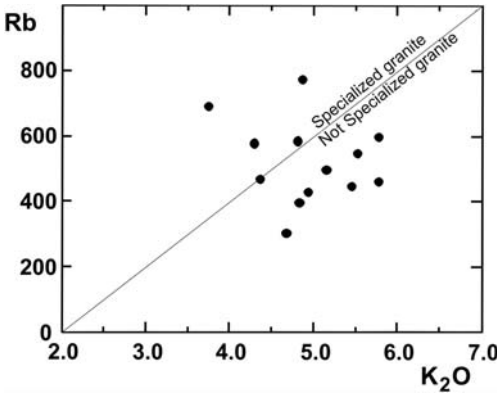

Fig. 5. Rb v. K_2O plot (Tuach *et al.* 1986) discriminating specialized and non-specialized granites.

the Sr/Eu ratio increases sympathetically with the evolution of the granitic magma.

The character of evolved granite is well illustrated in the Rb–Ba–Sr triangular diagram (El Bouseily & El Sokkary 1975). The plotted data points shift towards the Rb apex (Fig. 4a). A Rb–Ba–Cs complementary diagram (El Bouseily & El Sokkary 1975) distinguishes three fields: Ba decreases and Rb increases from field I to field III (Fig. 4b). Most samples in field III are Cs-enriched (mean 31.2 ppm) as those of field II (mean 26.9 ppm). Neiva (1984) had observed that samples within field III have the highest content of Sn (Sn $>$ 18 ppm) while samples within field II have Sn $>$ 15 ppm. In the present case, the situation is variable since the mean content of Sn within field III is 9 ppm, and in samples of field II, mean Sn is 15 ppm. Samples within field I belong to normal granites with average contents of Sn of 3 ppm (Fig. 4b) with regard to W, the samples within field II have a mean of 461 ppm and those of the field III have 328 ppm.

The Rb–K_2O diagram of Tuach *et al.* (1986) shows separate samples with the highest Sn and W contents belonging to the cupola zone (specialized granite) from those granites deeper, developed (not specialized granite), which indicates a geochemically layered pattern for the magmatic chamber (Fig. 5).

Main geochemical characteristics of the San Blas pluton are those of a fertile granite (with mean values of Sn = 13 ppm and W = 379 ppm), but the lack of ore veins and greisen in actual outcrops can be explained by a deep erosion of the granite cupola during the Carboniferous exhumation.

The diagram $CaO/(FeO + MgO + TiO_2)$ v. $CaO + FeO + MgO + TiO_2$ of Patiño Douce

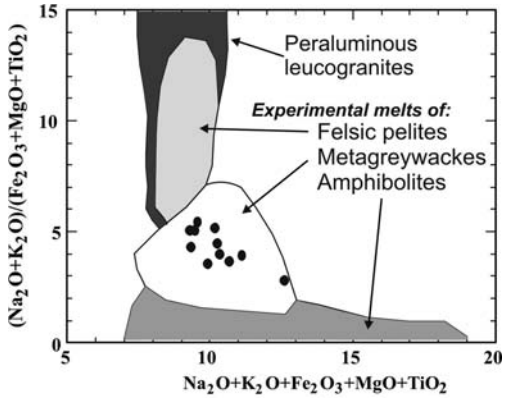

Fig. 6. Diagram $CaO/(FeO + MgO + TiO_2)$ v. $CaO + FeO + MgO + TiO_2$ (Patiño Douce 1999) which suggests a melt of crustal metagreywackes magma source.

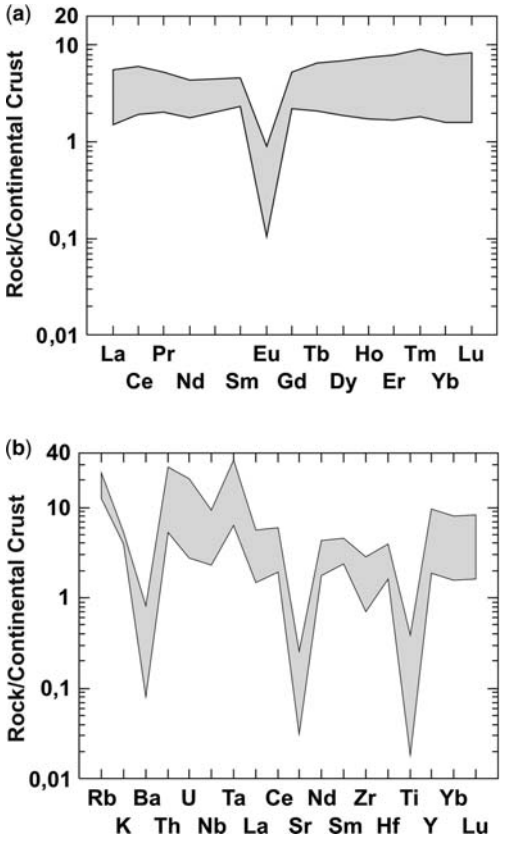

Fig. 7. (**a**) Continental crust-normalized REE patterns (Taylor & McLennan 1985), (**b**) Spidergram-normalized to continental crust values of Taylor & McLennan (1985).

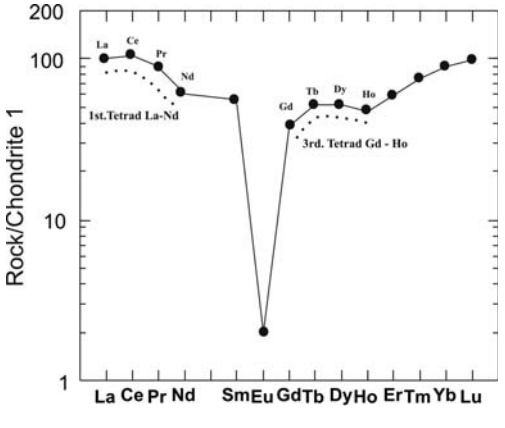

Fig. 8. Tetrad effect La–Nd (T_1), Nd–Gd (T_2), Gd–Ho (T_3), showed in sample 6515 from the San Blas pluton. Note the strong Eu negative anomaly.

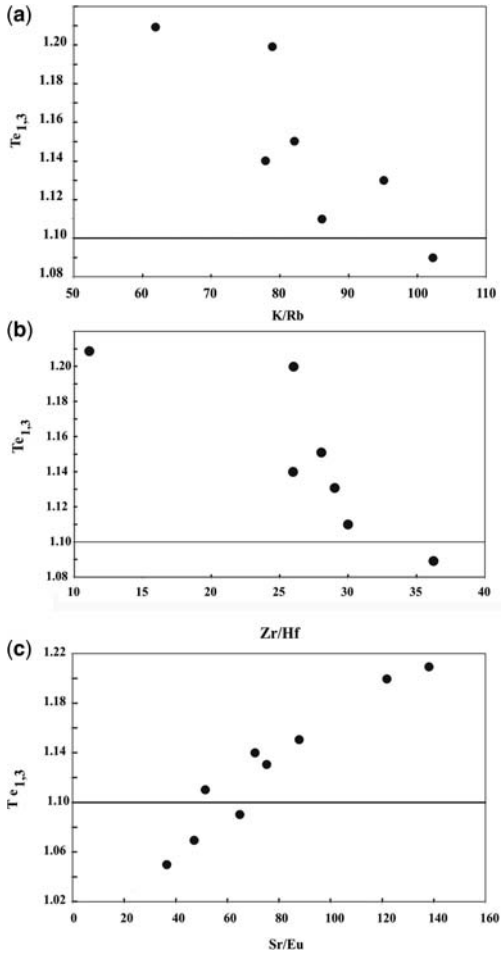

Fig. 9. (**a**) Tetrad effect plotted v. K/Rb, (**b**) Tetrad effect plotted v. Zr/Hf, (**c**) Tetrad effect plotted v. Sr/Eu. 1.1 is the minimum boundary for the tetrad effect.

(1999) shows evidence of a melt of crustal metagreywackes magma source. The experiments indicate that the metagreywackes contain biotite + plagioclase, but no aluminosilicates. The physical conditions of formation correspond to magmas formed by hybridization in continental crust of normal thickness at depths of 30 km or less (Fig. 6).

Continental crust-normalized REE patterns (according to Taylor & McLennan (1985) values) show remarkable negative Eu anomalies and flat patterns of distribution for the other REEs. These patterns suggest feldspar fractionation in the source (Fig. 7a).

Continental crust-normalized spidergrams (according to Taylor & McLennan (1985) values) show strong depletion of Ba, Sr and Ti. The depletion of Ba, Sr and Eu (in REE diagram) is

Table 3. *Values of the tetrad effect and ratios K/Rb; Sr/Eu; Zr/Hf and Eu/Eu**

Sample	$TE_{1,3}$	K/Rb	Sr/Eu	Zr/Hf	Eu/Eu*
5795	1.04	69	76	21	0.07
6445	1.14	78	70.7	26	0.44
6447	1.15	82	87.8	28	0.25
6452	1.09	102	65.5	36	0.16
6511	1.11	86	51.5	30	0.23
6513	1.20	79	122	26	0.23
6514	1.07	53	47	18	0.03
6515	1.21	62	138	11	0.04
6523	1.13	95	75	29	0.24
6749	1.08	45	–	15	0.15
6754	1.05	84	37	26	0.12
Average value	–	75	77	26	–

Table 4. *Data of Rb and Sr, in ppm*

Sample	Rb	Sr	$^{87}Rb/^{86}Sr$	Error	$^{87}Sr/^{86}Sr$	Error
6336	594	66	263 512	0.5270	0.830105	0.000032
6340	460	56	240 285	0.4806	0.820571	0.000027
6511	496	31	430 409	0.8608	0.909522	0.000049

not only originated by fractionation of feldspars but the effect is strongly enhanced by a late stage melt-fluid interaction. The spidergrams show also strong enrichment for Rb, Th, U, Nb, Ta and Y with respect to the continental crust; moreover Hf > Zr, and Rb > K. These enrichments can be explained by a late stage melt-fluid interaction, so high-field strength elements such as Nb, Ta, Zr, Hf, Y and REE may form complexes with a variety of bonds (F, B) whose stability is no longer constrained by the charge and ionic radius (Keppler 1993; Bau 1996) (Fig. 7b).

Some lanthanides in the San Blas granite show a 'tetrad effect', the most remarkable is shown in Figure 8. The tetrad effect was described for the first time by Fidelis & Siekierski (1966) and it is referred to a subdivision of the lanthanides in four groups, in a pattern of chondritic-normalized distribution: (1) La–Nd, (2) Pm–Gd, (3) Gd–Ho and (4) Er–Lu, and each group forms a convex pattern M-type (magmatic) or concave W-type (aqueous), (Masuda *et al.* (1987)). The four groups are separated in the boundary points located in between Nd and Pm, Gd, and in between Ho and Er, which correspond to a $\frac{1}{4}$, $\frac{1}{2}$, and $\frac{3}{4}$, filled 4f electronic shell.

The tetrad effect has been recognized in high evolved granitic rocks, hydrothermal alteration and mineralization. In the practice, only tetrads 1 and 3 are significant as shown in Figure 8.

The more evolved and those members with weak hydrothermal alteration (greisenization) in the San Blas pluton show a measurable tetrad effect. The measure of this effect is obtained by the mean deviation of the tetrad pattern with respect to the normal pattern of the REE without that effect. The first and the third tetrad have been obtained using Irber's (1999) formula. The data are shown in Table 2 and the results of the calculation in Table 3. Zr/Hf ratios in Table 2 are smaller than the chondritic ratio of 36.3 from Sun & McDonough (1989). That is a consequence of the larger solubility of $ZrSiO_4$ than $HfSiO_4$ in polymerized evolved meta- or peraluminous granitic melts, that results in a depletion of the Zr/Hf ratio (Linnen & Keppler 2002). The same conclusion was reached by Bea *et al.* (2006).

The tetrad effect ($Te_{1,3}$) must be higher than 1.1 for the reproduction of the characteristic pattern. ($Te_{1,3}$) was plotted against K/Rb, Zr/Hf and Sr/Eu (Fig. 9a–c). K/Rb and Zr/Hf ratios show negative correlation with the tetrad effect, while Sr/Eu ratio has positive correlation. The Eu/Eu* ratios are variable and show no correlation with the tetrad effect (Eu*, expected concentration from interpolating the normalized values of Sm and Gd). In spite of the weak tetrad effect, there is a correlation with the hydrothermal alteration shown by the rocks.

Isotopic geochemistry

Whole-rock Rb–Sr isotope data are presented in Table 4. The $^{87}Rb/^{86}Sr$ and $^{87}Sr/^{86}Sr$ of the three analysed samples define an isochron, obtained

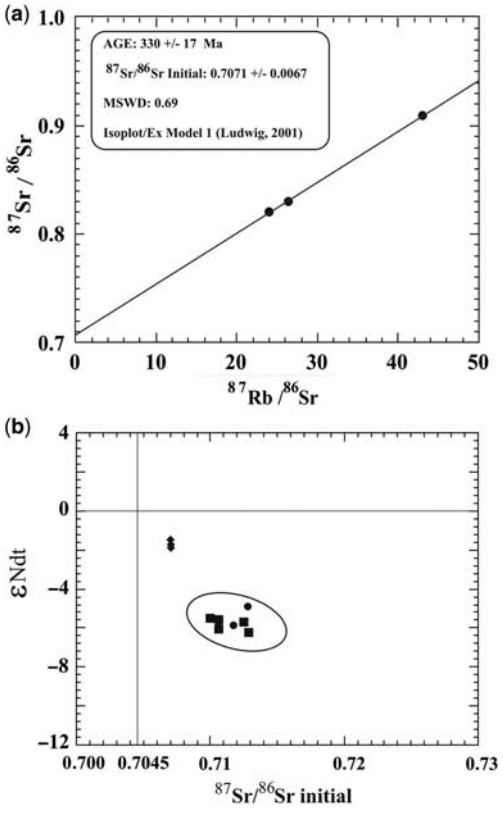

Fig. 10. (**a**) Rb–Sr Isochron for the San Blas pluton; (**b**) εNd_t v. $(^{87}Sr/^{86}Sr)_i$. Symbols: rhombs: San Blas granite; circles: Cerro Negro and Punta Negra Ordovician dacite porphyries (Toselli and Rossi, unpublished data); squares: Fiambalá and Copacabana Ordovician granitoids (Höckenreiner 2003); ellipse: Ordovician I and S granitoids (Pankhurst *et al.* 2000).

using the program Isoplot/Ex Model 1 (Ludwig 2001). The isochron yielded an age of 330 ± 17 Ma with an initial $^{87}Sr/^{86}Sr$ ratio of 0.7071 ± 0.0067 and MSWD 0.69 (Fig. 10a).

A previous age determination (U–Pb on zircon, TIMS technique) for the San Blas pluton indicated 334 ± 5 Ma (Báez & Basei 2005) and a U–Pb SHRIMP zircon age of 340 ± 3 Ma (Dahlquist *et al.* 2006).

The Sm and Nd whole-rock isotope analyses are shown in Table 5. Table 6 presents the Sm and Nd isotopic ratios for the samples, the chondritic uniform reservoir (CHUR), depleted mantle (DM) and continental crust (CC). The values of $(^{143}Nd/^{144}Nd)_{CHUR}$ are from Goldstein *et al.* (1984), $(^{147}Sm/^{144}Nd)_{CHUR}$ from Peucat *et al.* (1988), $(^{143}Nd/^{144}Nd)_{DM}$, $(^{147}Sm/^{144}Nd)_{DM}$ and $(^{147}Sm/^{144}Nd)_{CC}$ are from Liew & Hofmann (1988).

The data and isotopic two-stage model ages T_{DM} of 1,16–1,19 Ga, were obtained from Liew & Hofmann (1988) and the decay constant used: $\lambda_{Sm} = 6.54 \times 10^{-12} \times a^{-1}$. Figure 10b shows the plot of εNd_t v. $(^{87}Sr/^{86}Sr)_i$. Samples of the San Blas pluton plot on a restrict field with values of εNd_t between -1.3 to -1.8 and initial $(^{87}Sr/^{86}Sr)$ 0.707. The εNd_t and the model age T_{DM} data indicate that the petrogenesis of the San Blas granite involved a significant mantle component with an upper Mesoproterozoic crust. These data are different from those obtained for the Ordovician Famatinian granitoids whose εNd_t vary between -4 and -7, $(^{87}Sr/^{86}Sr)_i$ between 0.708 and 0.716 and their model age T_{DM}, between 1.5 and 1.7 Ga (Upper Palaeoproterozoic–Lower Mesoproterozoic) (Pankhurst *et al.* 2000; Höckenreiner 2003).

Table 5. *Data of Sm and Nd, in ppm*

Sample	Sm	Nd	$^{147}Sm/^{144}Nd$	$^{143}Nd/^{144}Nd$	Error 2σ
6336	11.40	53.70	0.1283	0.512398	0.000009
6340	8.60	45.70	0.1138	0.512364	0.000006
6511	9.60	39.52	0.1469	0.512452	0.000010

Table 6. *Isotopic ratios of Sm–Nd in the samples. Initial ratios of Nd isotope in the samples for t = 340 Ma, labelled εNd_t. CHUR, chondritic uniform reservoir; DM, depleted mantle; TDM, 2 stage model age.*

Sample	6336	6340	6511	CHUR	DM	Continental crust
$^{143}Nd/^{144}Nd$	0.512398	0.512364	0.512452	0.512638	0.513151	–
$^{147}Sm/^{144}Nd$	0.1283	0.1138	0.1469	0.1967	0.219	0.12
$(^{143}Nd/^{144}Nd)_t$	0.512120	0.512117	0.512144	0.512212	–	–
εNd_t	-1.79	-1.8	-1.3	–	–	–
T_{DM} (Ga)	1187	1190	1166	–	–	–

Discussion and conclusion

The geochronological data indicate that the San Blas granite is a Lower Carboniferous, undeformed pluton which intruded passively into Ordovician granitoids of variable grade of deformation. This fact makes this pluton equivalent in this aspect to other Carboniferous granites of the Sierra de Velasco (e.g. Huaco and Sanagasta plutons) (Toselli *et al.* 2006; Grosse *et al.* 2008, 2009; Söllner *et al.* 2007).

Plutons of this age are known in the northwestern Pampean Ranges, for example the La Quebrada pluton in Sierra de Mazan (Lazarte *et al.* 2006); Los Ratones and other minor bodies in the Sierra de Fiambalá (Arrospide 1985; Grissom *et al.* 1998; Lazarte *et al.* 2006); Papachacra granite in the Sierra de Papachacra (Lazarte *et al.* 2006) and in the Sierra de Zapata the Quimivil granite (Lazarte *et al.* 1999). With exception of Huaco and Sanagasta plutons, all the other above-mentioned plutons share common features with the San Blas granite in that they have geochemical signatures belonging to fertile granites with Sn and W mineralizations and constituting undeformed, nearly circular plutons, generally intruded into Ordovician granitoids with variable deformation grades, or as the case of the Los Ratones granite, intruded into a basement of low metamorphic grade and mylonite zones (Neugebauer 1995).

A remarkable characteristic of the Sierra de Velasco granites is a 'magmatic hiatus', namely, the absence of an intervening Devonian magmatism, with a gap of more than 100 Ma between the Ordovician and the Carboniferous magmatism. On the contrary, in the eastern and southern Pampean Ranges, Devonian granitic magmatism is dominant. It is recorded by large batholiths as Achala, Comechingones, Cerro Aspero-Alpa Corral, Córdoba province; and Las Chacras, Renca and others in the province of San Luis, while Ordovician batholiths are missing although abundant and voluminous to the north. Likewise in the south, there is a lack of Carboniferous granites, while in the north new Carboniferous granites have been discovered. The resolution of this important geological problem about the origin of the distribution timing of the plutonic magmatism during the Palaeozoic in the Pampean Ranges will be one of the main objectives of our future research.

The San Blas Carboniferous pluton is, for the moment, the only fertile granite in this area to which Sm–Nd model ages show participation of sharp different crustal–mantle sources. Future research should be extended to others Carboniferous granites, fertile or not, to find out if in their tectono-magmatic pattern, they share geological and genetic processes.

This research was supported by the Research Council of the National University of Tucumán and by the Superior Institute for Geological Correlation (INSUGEO). Special thanks go to the Institute of Geosciences of the University of São Paulo and to F. Söllner and P. Grosse, for isotope analyses at the Zentrallabor für Geochronologie, Munich, Germany. We thank two anonymous reviewers for their critical reviews and useful suggestions that have improved the manuscript.

References

Arrospide, A. 1985. Las manifestaciones de greissen en la Sierra de Fiambalá, Catamarca. *Revista de la Asociación Geológica Argentina*, **40**, 97–113.

Báez, M. A. 2006. *Geología, Petrología y Geoquímica del basamento igneo-metamórfico del sector norte de la Sierra de Velasco, Provincia de La Rioja. Facultad de Ciencias Exactas, Físicas y Naturales*. Universidad Nacional de Córdoba. PhD Thesis, National University of Córdoba, Argentina.

Báez, M. A. & Basei, M. A. 2005. El plutón San Blas, magmatismo postdeformacional carbonífero en la Sierra de Velasco. *Serie Correlación Geológica*, **19**, 239–246.

Bau, M. 1996. Controls on the fractionation of isovalent trace elements in magmatic and aqueous systems: evidence from Y/Ho, Zr/Hf, and lanthanide tetrad effect. *Contributions to Mineralogy and Petrology*, **123**, 323–333.

Bea, F. 1996. Residence of REE, Y, Th and U in granites and crustal protoliths; implications for the chemistry of crustal melts. *Journal of Petrology*, **37**, 521–552.

Bea, F., Montero, P. & Ortega, M. 2006. A LA-ICP-MS evaluation of Zr reservoirs in common crustal rocks: implications for Zr and Hf geochemistry, and zircon-forming processes. *The Canadian Mineralogist*, **44**, 693–714.

Clarke, D. B. 1992. The mineralogy of peraluminous granites: a review. *The Canadian Mineralogist*, **19**, 3–17.

Dahlquist, J. A., Pankhurst, R. J., Rapela, C. W., Casquet, C., Fanning, C. M., Alasino, P. H. & Báez, M. 2006. The San Blas pluton: an example of the carboniferous plutonism in the Sierras Pampeanas, Argentina. *Journal of South American Earth Sciences*, **20**, 341–350.

El Bouseily, A. M. & El Sokkary, A. A. 1975. The relation between Rb, Ba and Sr in granitic rocks. *Chemical Geology*, **16**, 207–219.

Fidelis, I. & Siekierski, S. 1966. The regularities in stability constants of some Rare Earth complexes. *Journal of Inorganic Nuclear Chemistry*, **28**, 185–188.

Goldstein, S. L., O'Nions, R. K. & Hamilton, P. J. 1984. A Sm–Nd study of atmospheric dusts and particulates from major river systems. *Earth and Planetary Science Letters*, **70**, 221–236.

Grissom, G. C., DeBari, S. M. & Snee, L. W. 1998. Geology of the Sierra de Fiambalá, northwest Argentina: implications for Early Palaeozoic Andean Tectonics. *In*: Pankhurst, R. J. & Rapela, C. W. (eds) *The Proto-Andean Margin of Gondwana*. Geological Society, London, Special Publications, **142**, 297–323.

Grosse, O., Báez, M. A., Toselli, A. J., Bellos, L. I., Rossi, J. N. & Sardi, F. G. 2008. Caracterización petrológica de los granitos Carboníferos (en contraposición con los granitoides Ordovícicos) de la Sierra de Velasco, Sierras Pampeanas. *Actas del XVII Congreso Geológico Argentino*, **III**, 1357–1358.

Grosse, P., Söllner, F., Báez, M. A., Toselli, A. J., Rossi, J. N. & de la Rosa, J. D. 2009. Lower Carboniferous post-orogenic granites in Central Eastern Sierra de Velasco, Sierras Pampeanas, Argentina: U–Pb monazite geochronology, geochemistry and Sr–Nd isotopes. *International Journal of Earth Sciences*, **98**, 1001–1025.

Höckenreiner, M. 2003. Die Tipa – Scherzone (Unterdevon, NW – Argentinien): Geochronologie, Geochemie und Strukturgeologie. *Münchner Geologische Hefte. Reihe A*, **34**, 1–92.

Irber, W. 1999. The lanthanide tetrad effect and its correlation with K/Rb, Eu/Eu*, Sr/Eu, Y/Ho and Zr/Hf of evolving peraluminous granite suites. *Geochimica et Cosmochimica Acta*, **63**, 489–508.

Jordan, T. E. & Allmendinger, R. W. 1986. The Sierras Pampeanas of Argentina: a modern analogue of rocky mountain foreland deformation. *American Journal of Science*, **286**, 737–764.

Keppler, H. 1993. Influence of fluorine on the enrichment of high field strength trace elements in granitic rocks. *Contributions to Mineralogy and Petrology*, **114**, 479–488.

Lannefors, N. A. 1929. Informe sobre las minas de estaño de Mazán y algunos otros trabajos mineros en la sierra de Velasco, Provincia de La Rioja. *Dirección General de Minas, Geología e Hidrología*, Buenos Aires, Publicación no 54..

Lazarte, J. E., Fernández Turiel, J. L., Guidi, F. & Medina, M. E. 1999. Los granitos Río Rodeo y Quimivil: dos etapas del magmatismo paleozoico de Sierras Pampeanas. *Revista de la Asociación Geológica Argentina*, **54**, 333–352.

Lazarte, J. E., Avila, J. C., Fogliata, A. S. & Gianfrancisco, M. 2006. Granitos evolucionados relacionados a mineralización estanno-wolframífera en Sierras Pampeanas Occidentales. *Serie Correlación Geológica*, **21**, 75–104.

Liew, T. C. & Hofmann, A. W. 1988. Precambrian crustal components, plutonic associations, plate environment of the Hercynian Fold Belt of Central Europe: indications from a Nd and Sr isotopic study. *Contributions to Mineralogy and Petrology*, **98**, 129–138.

Linnen, R. L. & Keppler, H. 2002. Melt composition control of Zr/Hf fractionation in magmatic processes. *Geochimica et Cosmochimica Acta*, **66**, 3293–3301.

Ludwig, K. R. 2001. *Using Isoplot/Ex Geochronological Toolkit for Microsoft Excel*. Berkeley Geochronological Center, Berkeley, Special Publication no. 1.

Maniar, P. D. & Piccoli, P. M. 1989. Tectonic discrimination of granitoids. *Geological Society of America Bulletin*, **101**, 635–643.

Masuda, A., Kawakami, O., Dohmoto, Y. & Takenaka, T. 1987. Lanthanide tetrad effects in nature: two mutually opposites types, W and M. *Geochemical Journal*, **21**, 119–124.

Neiva, A. M. R. 1984. Geochemistry of tin-bearing granitic rocks. *Chemical Geology*, **43**, 241–256.

Neugebauer, H. 1995. *Die Mylonite von Fiambalá – Strukturgeologische und petrographische Untersuchungen and der Ostgrenze des Famatina-Systems, Sierra de Fiambalá*, NW-Argentinien. PhD Thesis, Munich University, Munich.

Pankhurst, R. J., Rapela, C. W. & Fanning, C. M. 2000. Age and origin of coeval TTG, I- and S-type granites in the Famatinian belt of NW Argentina. *Transactions of the Royal Society of Edinburgh: Earth Sciences*, **91**, 151–168.

Patiño Douce, A. E. 1999. What do experiments tell us about the relative contributions of crust and mantle to the origin of granitic magmas. *In*: Castro, A., Fernández, C. & Vigneresse, J. L. (eds) *Understanding Granites: Integrating New and Classical Techniques*. Geological Society, London, Special Publications, **168**, 55–75.

Peucat, J. J., Vidal, P., Bernard-Griffiths, J. & Condie, K. C. 1988. Sr, Nd and Pb isotopic systematics in the Archean low- to high-grade transition zone of southern India: syn-accretion vs. post-accretion granulites. *Journal of Geology*, **97**, 537–550.

Söllner, F., Gerdes, A., Grosse, P. & Toselli, A. J. 2007. *U–Pb age determinations by LA-ICP-MS on zircons of the Huaco granite, Sierra de Velasco (NW-Argentina): A long-term history of melt activity within an igneous body*. Abstracts 20th Colloquium on Latin American Earth Sciences, Kiel.

Sun, S. S. & McDonough, W. F. 1989. Chemical and isotopic systematics of oceanic basalts: implications for mantle composition and processes. *In*: Saunders, A D. & Norrey, M. J. (eds) *Magmatism in Ocean Basins*. Geological Society of London, Special Publications, **42**, 313–345.

Taylor, S. R. & McLennan, S. M. 1985. *The Continental Crust: Its Composition and Evolution*. Blackwell, Oxford.

Toselli, A. J., Sial, A. N. & Rossi, J. N. 2002. Ordovician magmatism of the Sierras Pampeanas, Famatina System and Cordillera Oriental, NW Argentina. *In*: Aceñolaza, F. G. (ed.) *Aspects of the Ordovician System in Argentina*. Serie Correlación Geológica, Instituto Superior de Correlación Geológica, Tucumán, Argentina, **16**, 7–16.

Toselli, A. J., Rossi, J. N., Báez, M. A., Grosse, P. & Sardi, F. 2006. El batolito carbonífero Aimogasta, Sierra de Velasco, La Rioja, Argentina. *Serie Correlación Geológica*, **21**, 137–154.

Toselli, A. J., Miller, H., Aceñolaza, F. G., Rossi, J. N. & Söllner, F. 2007. The Sierra de Velasco of Northwest Argentina, Argentina. An example for polyphase magmatism at the margin of Gondwana. *Neues Jarhbuch für Geologisch und Paläontologisch Abhandlungen*, **246**, 325–345.

Tuach, J., Davenport, P. H., Dickson, W. L. & Strong, D. F. 1986. Geochemical trends in the Ackley Granite, southeast Newfoundland: their relevance to magmatic-metallogenic processes in high-silica systems. *Canadian Journal of Earth Sciences*, **23**, 747–765.